Thesis Paper

Injection and Evaporation of 100% methanol

C.J. van Iersel,Prof. dr. ir. R. G. van de Ketterij,Cdr. (ME) dr. ir. R. D. Geertsma,

Injection and Evaporation of 100% methanol*

C.J. van Iersel[a], Prof. dr. ir. R. G. van de Ketterij[b] and Cdr. (ME) dr. ir. R. D. Geertsma,[b,a]

[a]Delft University of Technology, Mekelweg 5, Delft, 2628 CD, The Netherlands
[b]Netherlands Defence Academy, Het Nieuwe Diep 8, Den Helder, 1781 AC, The Netherlands

ARTICLE INFO

Keywords:
injection
evaporation
methanol
port-fuel injection
spark-ignition
experiments
shadowgraphy

ABSTRACT

The use of methanol as a fuel alternative is considered one of the more promising options to be implemented in a relatively short to medium time frame; based on the potential availability, emission reduction, energy density, potential to be synthetically produced, scalability of production, and its implementation on board ships (both new build and retrofitted).

This paper investigates potential improvements of the injection system to achieve complete evaporation in the air inlet of a port-fuel injection engine to avoid wall-wetting of the scavenger air receiver and inlet valve. As a result, the methanol-air mixture in the cylinder would become more homogeneous and able to provide 100% of the rated engine power. Earlier research indicated that the wall-wetting fuel film and its evaporation rate directly affect the air-fuel ratio of the in-cylinder mixture, stability of the combustion process, and overall engine performance. The study includes the development of an injection model simulating low-pressure port-fuel injection, similar to the system fitted on our Caterpillar test engine, and the development of a single-droplet evaporation model to gain inside into the evaporation process of 100% methanol.

Based on the performed experimental research, we conclude the average droplet size ranges between 100 and 120µm. The average droplet speed was determined at ±35 m/s and the spray angle at 20°. At room temperature and pressure, the injection spray ended against the back-glass of the evaporation chamber, indicating almost none of the ethanol evaporates under these conditions. The injection length exceeds at least ±40 cm at atmospheric temperature and pressure, which is in line with the results of the single-droplet evaporation model.

1. Introduction: Moving away from fossil fuels

The maritime sector faces challenges in meeting the set goals in greenhouse gas reduction and lowering its climate footprint. According to UK Research and Innovation [1], the shipping industry is responsible for around 940 million tonnes of CO_2-emissions annually, around 2.5% of the world's total CO_2 emissions. At the same time, regulations regarding CO_2 and other greenhouse gas (GHG) emissions increase. The greenhouse gas regulations from the Paris Climate Accords and subsequent agreements of the International Maritime Organisation (IMO), strive to reduce CO_2-emissions by at least 40% by 2030, pursuing efforts towards 70% by 2050, compared to 2008; and to reduce the total annual GHG emissions from international shipping by at least 50% by 2050 compared to 2008 [2].

Part of the solution is to switch from fossil to non-fossil fuels produced with renewable or zero-carbon energy sources, requiring developments into new fuel types for the shipping industry are required [3]. Different shipping sectors have different preferences for their choice in fuel alternatives, both in the short and long term. For example, a ship operating on battery power is only useful when it is able to replenish within hours or days. For ships operating on hydrogen, this operational window is extended to approx. one week, while for methanol the operational window could be extended to approx. two weeks. In case longer operational windows are required, fossil or bio-fuel remains the main choice. In conclusion, autonomy is the key factor in the consideration which fuel alternative to use [4].

At this time, methanol as fuel alternative is considered as one of the more promising options ready for implementation in a relative short to medium time frame for ships requiring medium autonomy. This is based on the potential availability, emission reduction, energy density, potential to be synthetically produced, scalability of production, and implementation on board ships (both new-build and retrofitted). Van de Ketterij [5] argued that the use of fossil-based methanol as energy carrier could reduce Tank-to-Wake[1] CO_2-emissions by up to 10% compared to Marine Diesel Oil (MDO) and improve the air quality emissions such as SO_x, NO_x and PM. In addition, Well-to-Tank emissions and energy consumption are associated with the production, transportation, manufacturing and distribution of fuels. The Joint Research Centre of the European Commission provides a comprehensive overview for a large variety of fuels, and states that the production method and feedstock dominates the overall Well-to-Tank emissions of any bio- or synthetic fuel [7]. With use of renewable energy sources, the production of synthetic fuel could potentially reduce emissions up to 80% [8].

*Experimental and simulation-based research into the injection and evaporation of 100% methanol for use in a port-injected spark-ignited ICE

ORCID(s):

[1]The tank-to-wake approach solely looks at the emissions derived from on-board fuel combustion, referring only to the life cycle assessments of GHG emissions from the fuel in a ship's tank to the ship's exhaust [6]

2. Objective

The objective of this paper is to investigate how to improve the evaporation of methanol when injected in the air inlet receiver, in order to achieve complete evaporation of methanol before reaching the inlet valve. This would lead to a homogeneous methanol-air mixture in the cylinder that can provide 100% of rated engine power. We created an injection model for 100% methanol as fuel. Currently, no research has been found on the modelling of low-pressure injection valves for the use of methanol. Next, we created a single-droplet evaporation model especially created for the evaporation of 100% methanol. This single-droplet evaporation model involves the spray development, droplet formation, evaporation, and required heat of vaporisation of the injected methanol. Finally, an experimental setup was constructed to test various low-pressure injection nozzles at atmospheric pressure and temperature, as well as measure their individual spray characteristics and droplet size in those conditions.

3. Method

3.1. System Description

Originally, the Caterpillar G3508A test engine is a turbocharged spark-ignited natural gas engine with eight cylinders and a rated power of 500 kW at 1500 rpm, shown in Figure 1. The engine has been modified to run on methanol with the use of eight separate injection nozzles; each nozzle being installed off centre on the inlet air receiver of a cylinder, circled in red. Figure 2 and 3 show the arrangement of the inlet air receiver. Figure 3 shows the off-centre installation of the injection nozzle (blue arrow) – ±2.5 cm off-centre, and the location of the flame arrestor (red arrow). The inlet air receiver has a diameter of ±9 cm, and the injection nozzle is approx. 10 cm away from the end of the receiver. When the flame arrestor is installed inside the air receiver, the vertical distance reduces to approx. 7 cm. This is the distance available for the evaporation of the entire methanol spray from the nozzle, without the interference of any appendages.

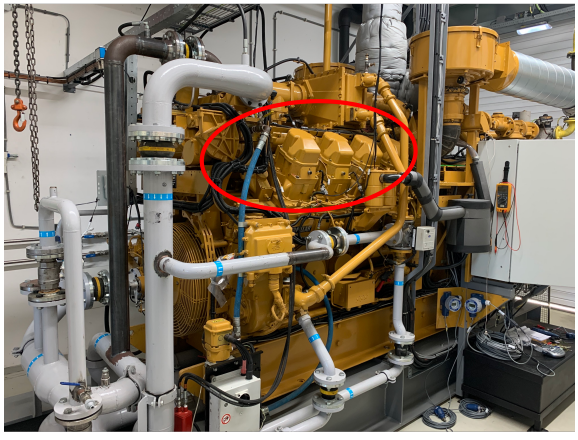

Figure 1: Caterpillar G3508A

Figure 2: Airflow through inlet air receiver [9]

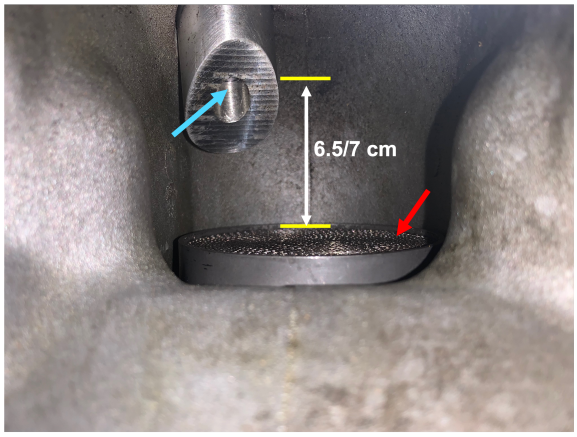

Figure 3: Arrangement of nozzle inside inlet air receiver [9]

3.2. Research structure

The research structure of this paper is visualised in Figure 4. The low-pressure injection model is created to obtain the injection pressure and volumetric flow rate, whereas the single-droplet evaporation model uses an estimated droplet size as input to simulate the evaporation rate of a single droplet. The low-pressure injection model and single-droplet evaporation model are both connected by the droplet size. The modelling of the spray characteristics (droplet size) was not included in this research. This made it necessary to perform experimental research to obtain a valid input of droplet size into the single-droplet evaporation model. Finally, a discussion is started that translates the findings of this paper and the real-time situation inside the engine. Followed by the conclusion and future research in improving the low-pressure injection model, single-droplet evaporation model, and custom-built experimental setup.

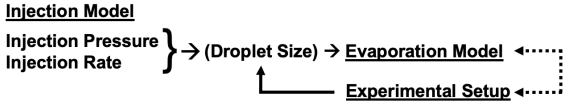

Figure 4: Research structure

4. Theoretical framework

4.1. Types of injection

Methanol can be injected in internal combustion engines in a number of ways. Because of its chemical properties, the cetane number is too low to allow compression ignition inside a standard compression ignition engine. The air-fuel mixture can be ignited either by using a spark, or by means of a pilot fuel. This results in the following options for the injection and ignition of methanol in an internal combustion engine [5]:

- Direct injection of methanol-diesel emulsifier blend
- Direct injection of methanol and separate pilot fuel injection
- Port-fuel injection of methanol and pilot fuel ignition
- Port-fuel injection and spark-ignition of methanol
- Combination of port-fuel injection and direct injection

When more than 50% of methanol is being injected into the scavenge air receiver, the process is referred to as major fraction port-fuel injection. Otherwise, it is called minor fraction port-fuel injection.

Direct injection of an emulsifier blend is the cheapest way to realise injection and ignition of methanol for existing compression ignition engines. This application requires the least amount of hardware changes to the fuel injection system, meaning that the normal injectors and fuel pipes could be used. However, the use of methanol-diesel emulsifier blends led to combustion problems at partial load and earlier breakdowns of rubber parts of the engine. Before injecting the methanol-diesel blend, it must be made sure that the mixture is stable and homogeneously mixed. Otherwise, ignition will fail if a pure methanol injection takes place [10]. Separate direct injection of allows methanol and pilot fuel to be injected separately and enabling the tuning of injection timing. This ignition method requires a significant reconstruction of existing engines. It would be necessary to add additional piping and an extra injection nozzle in the cylinder head. Smaller engines may not have sufficient space in the cylinder head for these two injection nozzles. This method therefore requires high investment costs for new parts and research into engine performance for direct injection CI engines [5, 10].

Methanol has a higher heat of vaporisation compared to diesel fuel. This may negatively influence the in-cylinder combustion process. To overcome this problem, methanol could be injected into the air inlet of the engine, giving the methanol droplets time to evaporate in the air. As a benefit, the methanol is already in a vapour phase when entering the cylinder. Moreover, the heat from the air after the turbocharger could be beneficially used. In case of port-fuel injection of methanol and pilot fuel ignition. Methanol is injected into the intake air stream and diesel pilot is injected directly into the cylinder to ignite the methanol-air mixture.

Port-fuel injection of methanol and pilot fuel ignition requires two separate injectors. A low-pressure injector located in the air inlet receiver and used for injecting the methanol and a high-pressure injector in the cylinder head used for the injection pilot fuel. In addition, a control system is required to control the methanol and pilot fuel injection quantity and timing, etc. A disadvantage of this method is the increase in net weight of the system, due to the additional fuel injection equipment required for the introduction of methanol [11, 12].

This paper looks at port-fuel injection of 100% methanol in a spark ignited engine. These engines use a spark plug to ignite the fuel inside the cylinder. This type of injection and ignition method is also utilised on the Caterpillar G3508A test-engine. A schematic overview of the port-fuel injection of methanol and spark-ignition is shown in Figure 5.

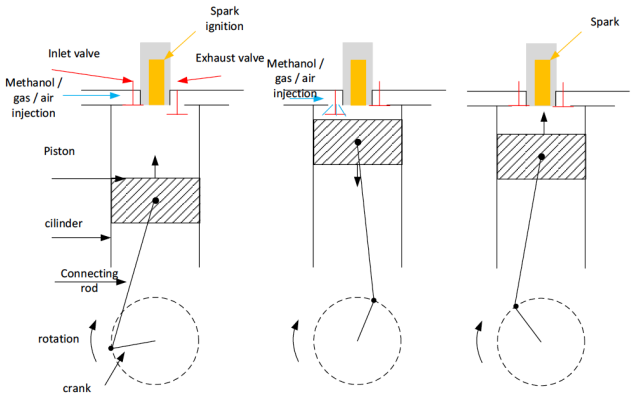

Figure 5: Schematic overview of the port-fuel injection of methanol and spark-ignition [5]

It is also possible to have a combination of both port-fuel and direct injection, making the engine independent of being spark-ignited or pilot fuel ignited. This could be done to improve the operability and response of the engine; especially in varying load conditions.

4.2. Spray characteristics and evaporation of methanol

During injection, as liquid jet of methanol leaves the nozzle it becomes turbulent and spreads out as it entrains and mixes with the surrounding air. The outer surface of the jet breaks up into droplets, while the liquid column leaving the nozzle disintegrates over a finite length into drops of different sizes, called the breakup length. As the liquid jet moves away from the nozzle, the mass of air within the spray increases. This causes the spray to diverge, increasing its width and decreasing its velocity. The methanol droplets evaporate as the air-entrainment process proceeds, where the droplets on the outer edge of the spray evaporate first, creating a fuel vapour-air mixture envelope around the liquid-containing core [13].

The atomisation of a liquid fuel is a very important process in engine combustion and emission formation. It is therefore important to understand the effect of methanol properties on the atomisation process. For port-fuel injection engines, methanol spray must be produced fine enough to enable a significant portion to evaporate and follow the airstream directly into the cylinder. In case of liquid impingement of fuel, where the fuel collides with the scavenge

air inlet, inlet valve, or cylinder wall, pollutant emissions and deterioration of the engine as a result of corrosion tend to be higher - impacting maintenance costs and increasing engine downtime. It is therefore essential to understand the fuel spray dynamics under realistic engine-like conditions.

Several studies have been performed on the evaporation of methanol spray characteristics [14, 15, 16, 17, 18, 19]. To summarise these studies, the following methods could improve the spray characteristics of methanol [9]. Firstly, a higher spray pressure decreases the formation period of spray and increases the penetration rate. Whilst a higher back-pressure inside the inlet manifold leads to the shrinkage of the spray angle [14]. Secondly, an increase in injection pressure results in a significant reduction in droplet size and enhanced atomisation for methanol sprays [15]. Thirdly, experimental research which varied the fuel temperature at constant ambient temperature showed that the flash-boiling sprays were able to increase the spray angle for rapid fuel–air mixing, and strongly improved the evaporation of the fuel spray [16]. It showed the important role between the ratio of ambient pressure and liquid saturation pressure during the spray flash boiling with good correlations to the spray characteristics. The structure of the flash boiling spray is dominated by the degree of superheat, denoted as the ambient-to-saturation pressure ratio. This degree of superheat is the difference in temperature between a superheated vapour and saturated vapour at the same pressure. Spray penetration, plume width and droplet size show a strong correlation with the ambient-to-saturation pressure ratio [17]. Fourthly, the ambient gas density has a significant effect on both methanol liquid and vapour penetration. Research found that an increase in ambient gas temperature significantly reduces the methanol liquid penetration, however, it has only a limited influence on the vapour penetration [18]. Finally, the droplet size of the injector could be further reduced using a custom air-assist injector cap, as shown by Dodge et al. [19]. The initial spray test measured an average droplet size of 116 µm for the 4-ms pulse width (idle condition) and 136 µm for the 10-ms pulse width (a higher power condition). After the initial test, their research used a custom air-assist injector cap to produce droplets with a cross-section average diameter of approx. 7.5 µm with fuel-injection pulse widths of 4 ms (idle condition) and average diameters of 9 µm with a 10-ms pulse width. These fine-spray droplets were small enough to follow the airstream past the intake valves and into the engine cylinders.

Subsequently, the evaporation process inside the scavenger air inlet could be improved in various ways. The studies state the following improvements [9]: An increase of the inlet air temperature improves the evaporation of the methanol spray. Heat transfer from the heated air to the droplet increases the internal temperature and therewith the fuel vapour pressure and evaporation rate, as stated by Heywood [13]. Zeng et al. [16] showed that flash-boiling sprays could result from increased fuel temperature or decreased ambient pressure. This resulted in much higher evaporation rate and increased spray angle for rapid fuel–air mixing. The use of fine-spray port-fuel injectors inside the scavenger air inlet must create spray droplets that are fine enough, approximately 20 µm in diameter or smaller, to stay suspended in the air and flow into the cylinder. This observation inspired Dodge et al. [19] to develop the air-assisted cap previously mentioned.

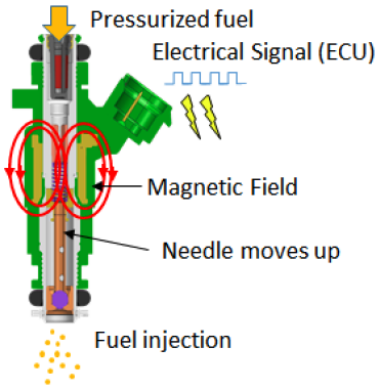

Figure 6: Working principle of PFI injector [20]

5. Injection Model

The development of the low-pressure injection model focused on reproducing the behaviour of an electrical injector used for port-fuel injection applications. This made three parameters especially important: the volumetric flow rate and pressure drop which the model provides, and the droplet distribution which is established experimentally.

5.1. Injector Configuration

Figure 6 shows the main components and working principle of low-pressure fuel injector. A filter strainer is placed in the fuel injector inlet to protect the other components of the injector against any contamination's. The fuel injector is energised by a voltage pulse. This generates a magnetic field (B) inside the coil and therefore a magnetic flux (ϕ), which pulls in the armature and lifts the needle of the valve seat. This movement allows fuel to flow through the fuel injector. When the coil is de-energised, the spring force and pressure force press the valve needle against the valve seat to seal the fuel-supply system from the intake manifold. The injected volume of fuel per time unit is determined by the system pressure and the available cross-section of the spray orifice in the orifices plate.

5.2. Modelling Methodology

The development of the one-dimensional simulation model aimed at outputs comparable to real-life measurements preformed by Ferreira et al. [20] on the performance of a fuel injector. As starting point, the so-called black box principle was implemented. The fuel injector was subdivided into three functional sub-groups, i.e. electric (magnetic), mechanic and hydraulic. Figure 7 illustrates each sub-group, all relevant inputs, outputs, and identifies the interaction between groups. The interaction between the segments can be summarised as a chain effect, starting at the solenoid controls, a force interaction, and the subsequent lifting of the needle valve.

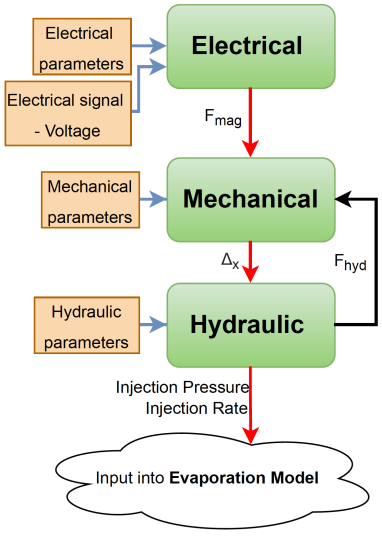

Figure 7: General overview of function groups [9]

Simplified Solenoid Model

The electric actuation block consists of a solenoid and magnetic force block. These two blocks calculate the magnetic force and control the injection timing of the injector. The magnetic force output initiates the needle displacement. The simplified solenoid model is based on the resistor–inductor circuit. In a resistor–inductor circuit, the current will not immediately rise to its maximum value when a voltage is applied, due to the presence of inductance. This results in a response delay, as is present in real solenoids. The differential equation corresponding to the transitory regime immediately after closing the resistor–inductor circuit is given by Eq. 1 [21]:

$$E - Ri - L\frac{di}{dt} = 0 \longrightarrow Ri + L\frac{di}{dt} = E \tag{1}$$

The current expression through the resistor–inductor circuit after closing is the solution of the differential equation of the circuit Eq. 1, shown by Eq. 2 [21].

$$i(t) = \frac{E}{R} \cdot \left(1 - e^{\left(-\frac{R}{L} \cdot t\right)}\right) \tag{2}$$

Valve Model

The mechanical valve block is modelled according to the principle of the mass–spring–damper system. The mathematical description of this mass–spring–damper function is shown in Eq. 3.

$$F_{mag} = F_m + F_p + F_s + F_d \longrightarrow F_m = F_{mag} - F_p - F_s - F_d \tag{3}$$

This equation of equilibrium (Eq. 3) is based on five forces. F_m is the resistance force or mass inertia ($m\ddot{x}$), F_d is the damping force of the needle, F_s is the spring force, F_p is the pressure/hydraulic force, and F_{mag} the electromagnetic force of the solenoid.
These forces are calculated as follows: The pressure or hydraulic force is calculated using Eq. 4.

$$F_p = (P_{rail} \cdot A_{in}) - (P_{manifold} \cdot A_{nozzle}) \tag{4}$$

Where, A_{in} is the cross area over the valve, P_{rail} is the rail pressure, A_{nozzle} the cross area under the valve, and $P_{manifold}$ is the inlet manifold pressure.

The spring force is calculated using Eq. 5.

$$F_s = K_{initial} + k \cdot x \tag{5}$$

Where, $K_{initial}$ is the initial tension of the spring, k is the spring stiffness, and x the displacement of the needle valve.

The damping force is calculated using Eq. 6.

$$F_d = b \cdot \ddot{x} \tag{6}$$

Where, b is the damper rating of the needle valve [N/(m/s)], and $\ddot{x}$ is the velocity of the needle valve.

The electromagnetic force is calculated using the following equation described by Szpica et al. [22]. The electromagnetic force being the result of the circuit operation can be obtained from the relation shown in Eq. 7.

$$F_{mag} = \frac{1}{2} I^2 \frac{dL(x)}{dx} \tag{7}$$

Where, I is the current and L is inductance.

By using Faraday's and Kirchhoff's laws, one may obtain a differential equation describing the change of the current supplying the electromagnetic circuit, as shown in Eq. 8.

$$\frac{dI}{dt} = \frac{1}{L(x)}\left(U - RI - \frac{dL(x)}{dx}\frac{dx}{dt}I\right) \tag{8}$$

Where, R is the resistance and U is the voltage.

Consequently, substituting Eq. 4 to 7 into the second-order differential equation of Eq. 3, which governs the dynamics of the needle valve, results in Eq. 9 shown below.

$$m \cdot \ddot{x} = \left[\frac{1}{2} I^2 \frac{dL(x)}{dx}\right] - \left[b \cdot \ddot{x}\right] - \left[K_{initial} + k \cdot x\right] - \left[(P_{rail} \cdot A_{in}) - (P_{manifold} \cdot A_{nozzle})\right] \tag{9}$$

Where, m is the mass of the needle valve; $\ddot{x}$, $\dot{x}$, and x the acceleration, velocity, and displacement of the needle valve respectively.

Injection Nozzle Model

The final sub-model calculates the injection rate and injection pressure over time; based on the needle displacement, manifold pressure, and pressure drop over time as its inputs. The volumetric flow rate of the methanol is calculated using Eq. 10.

$$Q_{inj} = \xi_n \cdot C_{d_{needle}} \cdot A_{nozzle} \cdot \sqrt{\frac{2}{\rho}\left|P_{drop} - P_{manifold}\right|} \tag{10}$$

Where, ξ_n is a binary number representing the opening of the nozzle determined by the needle lift; $C_{d_{needle}}$ is the discharge coefficient of the outlet orifice; A_{nozzle} is the area

of the outlet orifice of the injector; and P_{drop} and $P_{manifold}$ are the pressure drop and manifold pressure outside the injector respectively.

The pressure of the injection nozzle is calculated according Eq. 11, as described by Chung and Zeng respectively [23, 24]. In case there is no injection, the pressure inside the injector is equal to the rail pressure of the fuel pump. During injection, as fuel leaves the injector, the injection pressure decreases.

$$P_{inj} = \frac{K_f}{V} \cdot Q_{inj} \tag{11}$$

Where, K_f is the bulk modulus of methanol, V is the injection volume, and Q_{inj} is the previously calculated volumetric injection rate.

5.3. Simulation and Results

Figure 8 illustrates the simulation results of the low-pressure injection model. It visualises the needle valve displacement, injection pressure decrease, and volumetric flow rate of three pulses of 5 ms each. During each injection pulse, the initial pressure of 5 bar decreases with approximately 0.12 bar per pulse. The injection pressure is almost instantaneously restored to the initial rail pressure. The volumetric flow rate per pulse is approx. 33 cubic centimetres per pulse, and approx. 330 cc of fuel over a total injection time of 100 ms. This injection volume can be tuned by modifying the area of the needle holes. It can be concluded that the developed mathematical description allowed for the simulation of the injection process to obtain the volumetric flow rate and injection pressure. This volumetric flow rate is an important parameter, as it could be used as input for future spatial evaporation models.

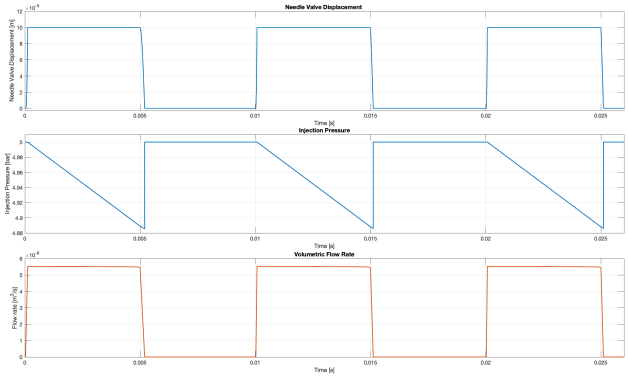

Figure 8: Simulation result of low-pressure injection system [9]

6. Evaporation Model

Droplet evaporation is of great importance for port-fuel injection applications, as time is very limited and conditions are relatively unfavourable for the evaporation.

6.1. Modelling

To investigate the effect of this evaporation process; the model considers a pure liquid droplet, suspended in an atmosphere of its own pure vapour, within a sufficiently large vessel and free from any external forces such as gravity. This assumption provided the basis of the single-droplet evaporation model and is based on a paper by Alroe et al. [25]. Because of the symmetry of a droplet, the physical scenario leads to a two-phase one-dimensional model, as shown in Figure 9.

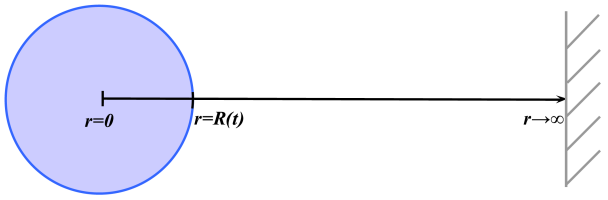

Figure 9: One-dimensional domain of droplet evaporation problem [25]

First, the systems of equations have to be established in each phase. In an attempt to account for all the relevant transport mechanisms, a "first principles" approach is taken to develop a model based on the fundamental conservation equations; the principles of conservation of continuity, momentum and energy. These conservation equations have been extensively covered by Bird, Stewart and Lightfoot [26]. Figure 10 shows an overview of the general conservation equations used by Alroe et al. [25] and during the modelling of this single-droplet evaporation model [9].

Continuity	$\frac{\partial \rho}{\partial t} = -\frac{1}{r^2}\frac{\partial(\rho r^2 V_r)}{\partial r}$
Momentum	$\rho\frac{\partial V}{\partial t} = -\nabla\cdot(\rho v^2) - \nabla p - [\nabla\cdot\tau]$
Energy	$\rho\hat{c_v}\frac{DT}{Dt} = -[\nabla\cdot q] - T\left(\frac{\partial p}{\partial T}\right)_{\hat{V}}(\nabla\cdot V) - (\tau : \nabla V)$

Figure 10: General conservation equations [26]

These general conservation equations were written in a system of equations outside the droplet and inside the droplet, based on spherical coordinates (r, θ, ϕ) and an ideal gas ($p = \rho T$). Outer boundary conditions were established to prevent any flows at the centre of the droplet, and Dirichlet boundary conditions were applied at the far vapour boundary, as it is sufficiently distant to be unaffected by the droplet over time ($r \to \infty$). In accord with derivations by Lock [27], boundary conditions are applied across the liquid/vapour interface. These boundary conditions enforce the continuity of temperature and mass, momentum, and energy flux. Collectively, these equations and boundary conditions form a closed system; however, solving such a highly coupled and non-linear system presents a challenging task, and made simplifications necessary. Firstly, it is assumed that the vapour can be modelled as an ideal gas and that the liquid is an in-compressible fluid. The former assumption removes vapour pressure from the list of parameters by relating it to density and temperature through the ideal gas law. This can be consider as a valid assumption, as the ideal gas law usually agrees with the behaviour of real gases to within 5% at normal temperature and pressure. At low temperatures or high pressures, real gases deviate significantly from ideal gas behaviour [28]. The in-compressible fluid assumption leads to three additional assumptions: constant liquid pressure, no mass flow within the droplet, and no viscous stresses

in either phase. As a result, both the conservation of mass and momentum equations can be eliminated from the liquid phase.

The temperature dependence of physical parameters was examined by Alroe et al. [25], such as the thermal conductivity, thermal diffusivity, and surface tension. In each case, for the relevant temperature ranges, the parameters did not vary significantly and were approximated as constants. After non-dimensionalising the system with the initial droplet radius set equal to one, the original system of equations was obtained. It demonstrated that the constants ν_{11} and the reciprocal of ν_2 were very small in comparison to the other proportionality constants. Approximating these two parameters are equal to zero, Alroe et al. [25] performed a perturbation analysis to identify the specific terms that had a negligible influence over the behaviour of the droplet. As a result, the constant $\frac{1}{\nu_2}$ in the conservation of momentum equation for the vapour phase implied that any change in the vapour pressure was insignificant. It reduced the conservation of momentum equation in the vapour phase to a simple statement of the isobaric condition. The second small coefficient, ν_{11}, is part of the inter-facial boundary condition. It was derived from the continuity of momentum and describes an equilibrium of forces at the interface. The negligible magnitude of ν_{11} implies a minimal contribution from vapour evaporating from the surface of the droplet.

Next, Alroe et al. [25] stated that it would be convenient to fix the moving interface by applying a spatial scaling to numerically solve the system. This involved a Landau scaling approach mentioned by Crank [29]. Although Landau scaling is ideal within the droplet itself, it is not within the vapour phase. As the droplet radius decreases due to evaporation, the Landau scaling progressively reduces the relative size of the vapour phase. This makes the Dirichlet boundary condition increasingly inaccurate. To maintain a fixed interface position, the following spatial translation in the vapour phase was applied.

$$r = x + R(t) - 1 \tag{12}$$

As a result of the simplifications and spatial transformations, the following reduced system of equations was obtained:

Liquid phase (Conservation of heat):

$$\frac{\partial T_l}{\partial \tau} = \frac{\dot{R}x}{R}\frac{\partial T_l}{\partial x} + \left(\frac{\nu_1}{R^2x^2}\right)\frac{\partial}{\partial x}\left[x^2\frac{\partial T_l}{\partial x}\right] \tag{13}$$

Vapour phase (Conservation of mass):

$$\frac{\partial}{\partial \tau}\left[\frac{1}{T_v}\right] = \dot{R}\frac{\partial}{\partial x}\left[\frac{1}{T_v}\right] - \frac{\nu_3}{(1+\nu_4)r^2}\frac{\partial}{\partial x}\left[\frac{r^2}{T_v}\frac{\partial T_v}{\partial x}\right] \tag{14}$$

Initial conditions:

$$T_l(x,0) = 1 \qquad T_v(x,0) = 1 \qquad R(0) = 1$$

Outer boundary conditions:

$$\frac{\partial T_l}{\partial x}(0,t) = 0 \qquad ; \qquad \lim_{x\to\infty} T_v(x,\tau) = 1 \tag{15}$$

Boundary conditions at the droplet surface:

$$T_l = \nu_5 T_v \quad ; \quad T_v = T_i \exp\left(\frac{\nu_{10}\sigma}{\nu_8\nu_9}\left(1 - \frac{1}{R}\right)\right) \tag{16}$$

$$\dot{R} = \frac{1}{\nu_7}\left(\nu_6\frac{\partial T_l}{\partial x} - \frac{\partial T_v}{\partial x}\right) ; T_i = \frac{L}{\widehat{R}}\left(\frac{T_b}{\frac{L}{\widehat{R}} - T_b\ln\left(\frac{p_v}{p_b}\right)}\right) \tag{17}$$

It is now possible to apply spatial and temporal discretisations to allow the reduced system to be solved numerically. As outlined by Patankar [30], these equations are well suited to a control volume scheme for spatial discretisation, due to their conservative nature. Alroe et al. [25] applied this technique to Eq. 13 by integrating across the control volume, which resulted in the following equation for the conservation of heat at the liquid phase:

$$\frac{\partial T_p}{\partial \tau} = \frac{3}{x_e^3 - x_w^3}\left[\frac{(x_e^4 - x_w^4)}{4}\frac{\dot{R}}{R}\frac{\partial T_p}{\partial x} + \frac{\nu_1}{R^2}\left(x_e^2\frac{\partial T_e}{\partial x} - x_w^2\frac{\partial T_w}{\partial x}\right)\right] \tag{18}$$

Where, the subscripts e and w refer to values at the east and west face of the control volume, and the p subscript refers to values at the central node. The non-linear terms were managed by assuming that the temporal derivative of T_l on the left hand side and the spatial derivative in the advective term were approximately constant across the control volume.

Next, temporal discretisation was applied by the integration of Eq. 18 over a discrete timestep with the use of the backward Euler, or implicit Euler, method to minimise any instability. The non-linearity in the advective term was managed by lagging the spatial derivative and using its value from the previous iteration.

$$T_p^{n+1} - T_p^n = \frac{3}{x_e^3 - x_w^3}\left[\frac{x_e^4 - x_w^4}{4}\frac{\partial T_p^m}{\partial x}\ln\left(\frac{R^{n+1}}{R^n}\right) \frac{\Delta\tau\ \nu_1}{(R^{n+1})^2}\left(x_e^2\frac{\partial T_e^{n+1}}{\partial x} - x_w^2\frac{\partial T_w^{n+1}}{\partial x}\right)\right] \tag{19}$$

Alroe et al. [25] applied a similar process to Eq. 14; however, the non-linearity within the diffusion term required the use of an averaging scheme and lagging. This resulted in the following equation for the conservation of mass at the vapour phase:

$$\frac{\partial}{\partial \tau}\left[\frac{1}{T_p}\right] = \dot{R}\frac{\partial}{\partial x}\left[\frac{1}{T_p}\right] - \frac{\nu_3}{(1+\nu_4)r^2}\frac{\partial}{\partial x}\left[\frac{r^2}{T_p}\frac{\partial T_p}{\partial x}\right] \tag{20}$$

$$\frac{1}{T_p^{n+1}} - \frac{1}{T_p^n} = \frac{\Delta\tau}{\partial x}\left[\left(\dot{R}\frac{\partial}{\partial x}\frac{1}{T_p}\right) - \frac{1}{r^2}\frac{\partial}{\partial x}\left(\frac{2\,\nu_3}{(1+\nu_4)}\frac{r^2}{T_p}\frac{\partial T_p}{\partial x}\right)\right] \tag{21}$$

Finally, these two equations (Eq. 19 and Eq. 21) were numerically solved using MATLAB. This numerical solver applied the Newton–Raphson method to iteratively solve for droplet radius and temperature at each timestep. This resulted in an efficient, stable convergence of the solution at each timestep.

6.2. Simulation and Results

The model needs to behave similar to established rules of droplet evaporation. In particular, it needs to follow the D^2-law, as discussed by McGaughey et al. [31] and Dodge et al. [19]. The law predicts that the square of the droplet diameter will change linearly over time. This D^2-behaviour is investigated using an initial simulated droplet evaporation. For this simulation, an initial droplet size diameter of 100 µm is used. The temperature of the methanol is set at 15°C, while the air temperature is set at 50°C. Lastly, the ratio partial pressure of methanol vapour at interface is set at 0.211%. This value represents the ratio between partial pressure of methanol over the saturated vapour pressure at variable temperature conditions. The saturated vapour pressure of methanol is determined using the Antoine equation, while the actual partial pressure of methanol is determined using a look-up table for the specific air temperature, volume, injector type, and specific injection timing. Figure 11 and Figure 12 show that there is a complete droplet evaporation (100 µm diameter) within one second (860 ms) and the square of the droplet diameter closely approximates the linear trend. This provides support for the model to follow the D^2-law.

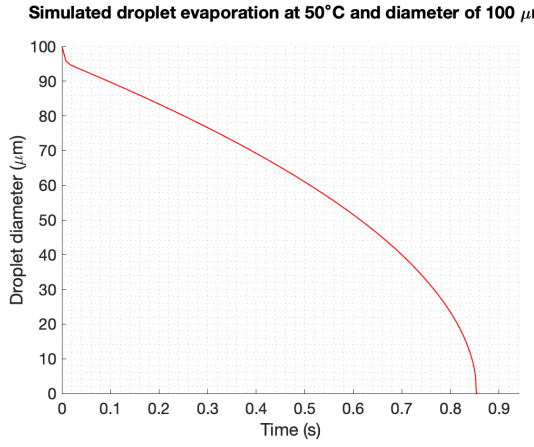

Figure 11: Droplet evaporation simulation at 50°C

Next, the evolution of the temperature profiles in the vicinity of the liquid/vapour interface is examined. Figure 13 shows the temperature throughout the liquid phase. It indicates that the liquid phase requires less than 90 ms to reach the same level as the interface. At this point, the entire liquid phase has a uniform temperature, approx. -50°C. Thus, no heat flow can occur from the interface into the liquid. However, the steep temperature gradients in the vapour phase guarantees heat flow from the vapour phase into the interface. In order to avoid violating the conservation of energy equation, it is necessary for the interface to move left into the liquid phase. This clearly shows that the imbalance in heat flux is the driving mechanism behind

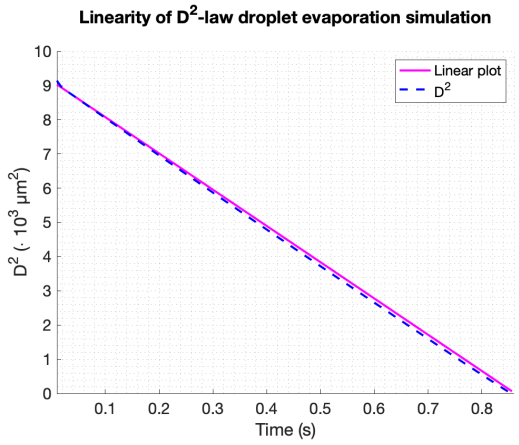

Figure 12: Comparison of D^2-law to an arbitrary linear function

the evaporation process [25]. Figure 13 assumes the most extreme and ideal situation at the liquid-vapour interface achievable. Thus, some important boundary conditions must be explained. The model considers a pure liquid droplet suspended in an atmosphere of its own pure vapour, where the ratio of partial pressure of methanol vapour is calculated and set as a constant of 0.211%; only considering the partial pressure of methanol and no other substances e.g., water vapour. The ratio directly outside the interface is kept constant during the evaporation of the droplet (so a simplification of reality). It results in the steep temperature drop to -50°C at the interface at the start of evaporation, from +50°C at an infinite distance away from the droplet. It must also be noted that the temperature at an infinite distance from the droplet remains equal to the set parameter of 50°C. The temperature decrease was not implemented into the model and will remain constant. Subsequently, the temperature decrease of the liquid phase is consistent with theory described by Heywood [13]. He uses the steady-flow energy equation for a constant-pressure flow with liquid fuel evaporation and with heat transfer. Heywood states that if no heat transfer to the mixture occurs, the mixture temperature decreases as liquid fuel is vaporised. For the complete evaporation of methanol and using an equivalence ratio (ϕ) of one, i.e the ratio of the actual fuel-air ratio to the stoichiometric ratio, the value $T_A - T_B$ would be -128°C, compared to for instance iso-octane which has a $T_A - T_B$ of -19°C; where, T_B is the temperature before evaporation and T_A after evaporation. In practice, heating occurs and the methanol is not necessarily fully evaporated prior to entry into the cylinder [13]. It could therefore be discussed that the temperature decrease to approx. -50°C, creating a ΔT of -100°C, is physically possible under these specific boundary conditions.

Investigating the response to changing conditions, three sets of simulations are performed. It uses the same initial temperature conditions, but with three different droplet size diameters (100 µm, 50 µm and 25 µm), and with a varying partial pressure ratio of methanol vapour at the interface; at the start of injection (no methanol present), halfway, and at the end of injection. Figure 14 depicts the simulations at 50°C. It clearly indicates that with an increasing partial

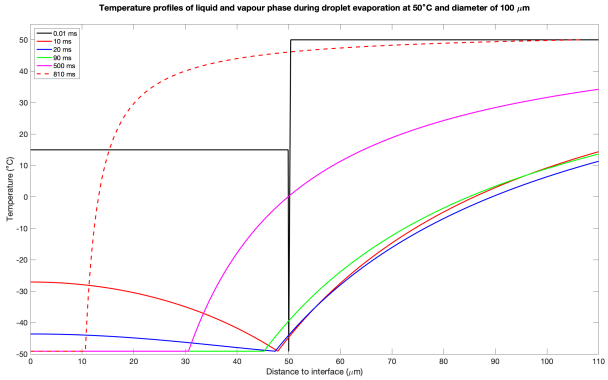

Figure 13: Temperature profiles near liquid-vapour interface

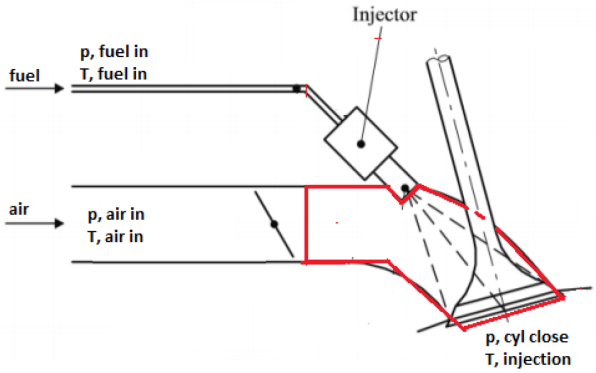

Figure 15: General arrangement of inlet air receiver [11]

pressure ratio of methanol vapour, the evaporation rate slows down. Based on the performed simulation, it can be concluded that with an increasing temperature and decreasing droplet diameter the evaporation rate of a single-droplet increases, i.e. the droplet evaporates faster. Figure 14 shows that with an air temperature of 50°C and droplet diameter of 100 µm, the evaporation of a single droplet takes between 1800 and 860 ms. This reduces to between 480 and 210 ms with a droplet diameter of 50 µm, and between 110 and 50 ms with a droplet diameter of 25 µm. To conclude, smaller droplets and a higher temperature result in a faster evaporation process. For the single-droplet evaporation model, it indicates that the droplet size, scavenger air temperature and liquid temperature, and the partial pressure ratio are the only parameters that have a significant effect on the evaporation rate. However, some parameters have a greater impact to the evaporation rate compared to others [9].

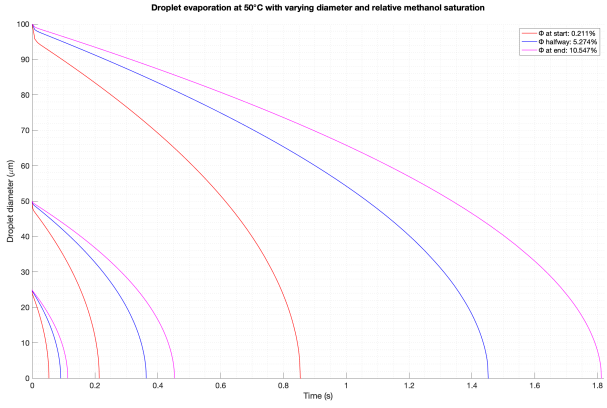

Figure 14: Droplet evaporation at 50°C with varying diameter and relative methanol saturation

7. Experimental Research

For this research, a custom-built experimental setup is constructed to test various low-pressure injection nozzles at atmospheric pressure and temperature, as well as measure their individual spray characteristics and droplet size in those conditions using the shadowgraphy technique.

7.1. Experimental Setup

The setup consists of three sub-systems; an evaporation chamber, a fuel system and injector, and an electronic control system. It tries to mimic the inlet air receiver of the Caterpillar G3508A test-engine, as shown in red in Figure 15. However, the conditions of the experiment vary with those in the inlet air receiver. The tests are performed at atmospheric pressure and air temperature, without any airflow, and inside an evaporation chamber volume which is larger than the inlet air receiver.

Evaporation chamber

The evaporation chamber is a transparent plastic box; having a length of 40.5 cm, a width of 25.7 cm, and a height of 22 cm, where the injector is installed longitudinally to the chamber. A top cover was manufactured and fixed using twelve bolts and a gasket, making the evaporation chamber "airtight" from the environment.

Fuel system

In order to supply the injector with sufficient fuel, a separate fuel system is constructed. The fuel system consists of six different components: a injector, a pressure regulator and pressure transmitter, a fuel pump, a portable balance, and fuel tank. The fuel tank is positioned on top of a portable balance, to measure the exact amount of fuel being injected into the evaporation chamber. As fuel pump, the Bosch FP165 inline roller cell pump was used. It is capable of providing 165 l/h at 5 bar, but the delivery volume can be tuned by changing the operating voltage, at a constant delivery pressure. After the fuel pump, the fuel is delivered to a three-way fuel pressure regulator. It ensures a constant fuel pressure to the injector and a continuous flow to cool the pump. The fuel pressure regulator is tuned to deliver 5 bar of pressure to the injector, any over-pressure is discharged along a return-line back to the fuel tank. The fuel pressure is measured using a pressure transmitter installed after the regulator. Finally, the Bosch EV14 injector is supplied with fuel.

Electronic control system

The electronic control system is required to operate the injector. This electrical signal actuates the solenoid coil and consists of a period and time of injection. The time of injection is the time the needle valve should be open for the passage of fuel, also known as the pulse width. The period (T) is the time it taken to complete one cycle. A pulse generator is used to tune the time of injection by modifying the pulse width, as it is a percentage of the period (T).

8. Post-processing and Results

After preforming the measurements, the data is post-processed. Unfortunately, the current setup did not allow the ethanol spray to evaporate within the evaporation chamber, resulting in a spray to the back-glass of the chamber. It is assumed that this lack of evaporation is caused by the very low atmospheric temperature inside the room. This is expected as the simulated evaporation of a single-droplet of 100 µm in ambient conditions (20°C and atmospheric pressure) takes approx. 980 ms, while the droplet travels across the entire evaporation chamber in approx. 11 ms.

Using the post-processed data, it is possible to investigate the droplet size, droplet speed, and overall spray pattern generated by the injection nozzle. Analysing the spray jet between 0-10 cm, MATLAB was able to execute a droplet search to detect more circular objects. Two different circle radii thresholds were used during the radius search; the first search was set between a circle radius of 5 and 20 pixels, resulting in a total droplet count of 2054 droplets. The second search was set between a circle radius of 1 and 8 pixels, resulting in a total droplet count of 4246 droplets. It must be noted that this count is not an accurate representation of the total amount of droplets in the spray jet, due to the fact a large part of the picture is out of focus. Thus, more droplets are present in the total spray jet as counted.

Based on the post-processed photograph, the average droplet size and average droplet speed are determined. The average droplet size is determined by counting the average amount of pixels for each single droplet and multiplying this with the specific scale of the photograph. It concludes that the average droplet size is between 100 and 120µm, with some droplets exceeding 130µm. The average droplet speed is determined at 35.6 m/s, by using the equation for dynamic pressure [32].

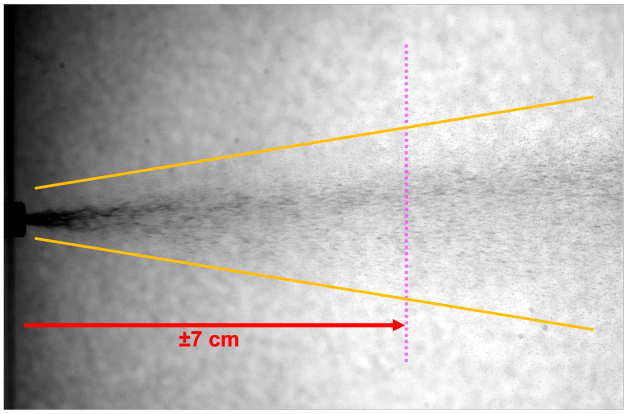

Figure 16: Overall spray pattern generated by nozzle [9]

Subsequently, the overall spray pattern generated by the injection nozzle is examined. This overall spray pattern gives an inside into the overall structure, injection and breakup length, droplet distribution, and spray angle. Figure 16 shows that the spray diverges away from the nozzle. Based on the literature, the figure confirms the statement that as one moves away from the nozzle, the mass of air within the spray increases, the spray diverges, its width increases, and the spray velocity decreases [13]. It distinguished the liquid-containing core of the jet and the extent of the droplet region of the spray which surrounds the liquid core. This droplet region contains the droplet size distribution of the spray, clearly visualising that more droplets are formed further away from the liquid core as the overall spray velocity decreases. The spray angle (α) is defined as the angle the jet forms at the moment when it leaves the nozzle orifice. This spray angle was determined to be 20° which corresponds by with the data sheet of the Bosch EV14 injector valve. The breakup length is defined as a liquid column that disintegrates over a finite length into different droplet sizes. It is divided into a primary and secondary breakup. The primary breakup length is the distance between the nozzle and the disintegration of the liquid sheet into ligaments; the secondary breakup length is the distance between the disintegration of the ligaments into droplets. Lastly, the injection length of the spray is determined. This length is defined as the distance along the spray axis to the boundary of the spray. Based on the performed experiments, the injection spray ended against the back-glass of the evaporation chamber. It can be stated that the injection length exceeds at least the ±40 cm at atmospheric temperature and pressure.

It was also possible to calculate the horizontal distance a droplet travels, assuming a laminar flow and neglecting its vertical component. This calculation assumed Stokes flow, where the Reynolds number was less than one and thus the particle drag coefficient was inversely proportional to the Reynolds number itself [32, 33]. Based on this calculation, it can be stated that a droplet of 100 µm diameter travels a horizontal distance of approximately 85 cm, assuming a laminar flow. In order to check whether the laminar flow assumption is justified for every droplet, the laminar flow required a low Reynolds number. At the start of injection, the highest Reynolds number for a droplet is realised, as here the higher velocity is present [32, 33]. This Reynolds number is calculated as $Re = 233.3333$. The Reynolds number for laminar flows is used to calculate the drag coefficient (C_D), which results in a value of 0.103. When this Reynolds number is compared to that of the drag coefficient for a sphere, as obtained from laboratory experiments, gives a C_D value of 0.722. It can be seen that the resistance from the laboratory experiments is higher than the resistance according to the equation for laminar flow. This means that the actual resistance is higher and that the estimated distance is therefore an upper limit. For the first droplet, the laminar assumption will give a reasonable estimate. However, for the second droplet this difference will be much larger. Thus, making this laminar assumption incorrect [33].

9. Discussion

Consequently, a discussion can be started based on the results of this paper and its translation to the real-time situation inside the engine. Especially, the results of the experiment and its influence on the engine regarding the lack of space in the inlet manifold. As a result, the following three questions need to be answered:

1. What could be concluded from the experimental research?
2. How could this be linked to the engine itself?
3. What could/should be improved to obtain better results during future (full-scale) experiments?

First, based on the experimental research, it became clear that the current setup did not allow the ethanol spray to evaporate within the evaporation chamber, as the injection spray hit the back-glass of the chamber. Using the post-processed data, we could conclude that the average droplet size is between 100 and 120 µm. The average droplet speed is determined at approx. 35 m/s, and the spray angle at 20°. The injection length exceeded at least the ±40 cm at atmospheric temperature and pressure, which does not contradict the results of single-droplet evaporation model. In addition, calculations regarding the injection length determine a maximum horizontal droplet distance of approximately 85 cm when assuming a laminar flow and neglecting its vertical component.

Second, the above mentioned results can be linked to the engine itself. The overall vertical distance available for the entire evaporation of methanol was determined at approx. 7 cm, as shown in Figure 3. Based on the performed experimental tests, it could be discussed that the tested injection nozzle did not sufficiently perform under atmospheric temperature and pressure, as the methanol jet would have hit the inlet valve. However, the tested atmospheric conditions of the experiment do not represent those in the scavenger air manifold and engine when operating. Based on recent trial runs with the Caterpillar G3508A engine, air temperatures were estimated between 50 and 70°C after the intercooler. The effects of these higher temperatures on the actual injection length and evaporation rate inside the engine are still to be determined. The simulated droplet evaporation rate of a 100 µm droplet is determined at 860 ms at an air temperature of 50°C, compared to 1.1 seconds at an air temperature of 20°C. It can be concluded that this evaporation rate is insufficient when operating the Caterpillar G3508A engine, due to the limited time available for the injection and evaporation of methanol. As a result, based on the theoretical framework, small droplet sizes and/or higher air temperatures can result in the faster evaporation rate of the methanol inside the scavenger air manifold. Consequently, future research must determine whether these higher air temperatures and/or smaller droplet sizes are sufficiently enough to evaporate all injected methanol within the available space of ±7 cm.

Third, in order to obtain better results during future (full-scale) experiments and measurements, the following improvements are discussed to be implemented and/or researched. The first improvement is based on the single-droplet evaporation model. It could be discussed that the single-droplet assumption is not consistent with the actual inlet manifold conditions, i.e. the spray pattern of the Bosch EV14 injection valves. This leads to the limitation that the single-droplet evaporation model is inadequate compared to the actual injection spray consisting of multiple droplets. A more detailed Computational Fluid Dynamics (CFD) model is required to further investigate the evaporation process. This CFD model would be beneficial in obtaining a more detailed overview of the generated spray pattern and its influence on the multi-droplet evaporation process. The second improvement is based on the custom air-assist injector cap. It will be necessary to validate the claim by Dodge et al. [19], stating that the droplet size of the injector could be further reduced using a custom air-assist injector cap. The necessity in validating this claim would be beneficial in obtaining smaller droplets using the standard Bosch EV14 injection valve. The third improvement is based on the Bosch EV14 injection valves. Currently, the tested Bosch EV14 injection valves have maximum flow rates which are inadequate to operate the Caterpillar engine at full load and one single injector per cylinder. Future research must therefore be performed in finding injection valves that create droplets with diameter smaller than 100 µm, but still injects sufficient amounts of fuel to operate the engine. The last improvement is based on the experimental setup. It can be discussed that the current experimental setup is not consistent with the actual inlet manifold conditions, as the experimental setup works at atmospheric pressure and temperature. This leads to the discussion that a more advanced setup is required to experiment with the injection valves. In order to gain inside into the jet spray generated by the nozzle at higher pressures and the subsequent evaporation process at higher temperatures.

10. Conclusion

Injection, atomisation, and evaporation are important processes in the combustion and emission formation of an internal combustion engine. Previous research showed that the wall-wetting fuel film mass and its evaporation rate directly affect the air-fuel ratio of in-cylinder mixture, as well as the performance of the engine itself.

Although the spray characteristics of methanol can be improved in various ways. It could be concluded that the important factors for atomisation inside the engine, i.e. a smaller droplet size, could be best achieved either by higher injection pressure or by use of the custom air-assist injector cap [14, 15, 18, 19]. The evaporation process of methanol inside the scavenger air inlet could be improved by higher inlet air temperatures and smaller droplets. These have the greatest effect on the evaporation rate according to the theoretical framework [13, 19].

The development of the one-dimensional simulation model of a low-pressure injector was focused on reproducing the behaviour of an electrical injector used for port-fuel injection applications. The model is based on a mathematical description of a simplified solenoid valve and mass-spring-damper system and consists of three sub-models. It can be concluded that the developed mathematical description allowed for the simulation of the injection process to obtain the volumetric flow rate and injection pressure, which are important inputs for future spatial evaporation models and represent that of the Caterpillar G3508A test-engine.

Next, an one-dimensional mathematical single-droplet evaporation model for the evaporation of methanol droplets was developed. To investigate the effect of this evaporation process, the model assumed a pure liquid droplet suspended in its own vapour. In an attempt to account for all relevant transport mechanisms, a "first principles" approach was taken by developing the model from fundamental conservation equations. The model required a limited set of assumptions to assist with the numerical analysis. It demonstrated a realistic response to the temperature, droplet size, and ratio partial pressure over the saturated vapour pressure, while consistently following the D^2-law to validate the model.

From the evaporation model, it was concluded that with an increased temperature and decreased droplet diameter the time of evaporation for a single-droplet decreased. This conclusion was already discovered in the theoretical background, but is now visualised and verified with the evaporation model. For this reason, smaller droplet diameters are required in case of engine-like conditions, preferably less than 20 µm, and the temperature needs to be sufficient for fast evaporation. The exact temperature could not be investigated, as the heat transfer from inlet air and hot engine parts to methanol liquid and vapour were not included into the model. For this spatial (CFD) analysis would be required, that could use the mechanism of this developed single-droplet evaporation model.

The custom-built experimental setup was able to test various low-pressure injection nozzles at atmospheric pressure and temperature and measure their individual spray characteristics and droplet size using the shadowgraphy measuring technique. The measurements taken by the experimental setup could not be used to establish the evaporation rates, also, because the evaporation at ambient conditions was very slow. This was expected as the simulated evaporation of a single-droplet of 100 µm in ambient conditions took approx. 980 ms, while the droplet travels across the entire evaporation chamber in approx. 11 ms. However, the current setup could be used to investigate how smaller droplet sizes can be achieved. For evaporation rate experiments, more engine-like conditions are required.

11. Future research

Based on the performed research, the following recommendations can be given on the future work into methanol as a fuel alternative for the maritime sector [9]. Additional research is required into improving the injector spray characteristics. In order to validate if an increase in spray pressure, higher ambient gas temperatures, and higher back-pressure indeed result in a reduction of droplet size and enhanced atomisation of methanol sprays. This could be checked by means of experimental tests, varying the spray pressure and temperatures. Secondly, it will be necessary to validate the claim by Dodge et al. [19], stating that the droplet size of the injector could be further reduced using a custom air-assist injector cap and improving the evaporation of the spray. This could be done by manufacturing a replica of the used air-assist injector cap and checking whether similar results are generated in an experimental setup. Thirdly, additional research is required in validating if an increase in inlet air temperature and back-pressure result in an improved evaporation of the methanol spray. For this a more advanced setup is required that could measure the spray and evaporation in engine-like conditions, such as 3 bar charge pressure and 50 to 90°C inlet air temperature.

An important recommendation regarding the injection model is the spray rate characteristic, which could be used as an input for CFD analysis for the evaporation and combustion of methanol. This additional research entails the spray characteristic, to obtain a simulated spray rate, spray pattern, and droplet size generated by the nozzle tip. Moreover, the low-pressure injection model has not been validated due to a lack of available time and resources. Further research is therefore essential to validate the generated results and improve upon the model's accuracy.

The most important recommendation is to extend the modelling framework of the single-droplet evaporation model. It would result in the next step to include the heat transfer between the methanol droplet, liquid/vapour interface, and the surrounding air and hot engine parts, as this would directly influence evaporation process. The current single-droplet evaporation model is too limited in its ability to display the engine-like evaporation process. A switch to Computational Fluid Dynamics (CFD) modelling is therefore recommended to further investigate the evaporation process in more detail. In addition, the model assumes the most extreme and ideal situation at the liquid-vapour interface. It considers a constant vapour ratio directly outside of the interface, which does not vary during the evaporation of the droplet. This assumption is a strong simplification considering the real-life situation, whereby the vapour ratio increases over time during the evaporation process (as a function of the distance from the interface of the droplet) and partial pressures of for example water vapour plays a role. It is therefore recommended to improve upon this process analytically by considering multiple layers of increasing vapour ratios around the droplet. This would simulate the evaporation process over time and its impact on the temperature profiles.

An important recommendation is additional research into the spray characteristics of methanol at low-pressure injection. The current experimental setup is very useful for the evaluation of spray formation, droplet size distribution in the spray, and flow rate of the injector. These parameters are a crucial starting point for spatial CFD evaporation modelling. It would be necessary to visualise the spray characteristics and determine the (initial) droplet sizes at various pressures, temperatures, and distances along the spray length. It is therefore recommended to obtain a more advanced experimental setup that could measure the spray and evaporation in engine-like conditions. Especially, the impact of the injection pressure, higher manifold charge pressure, and higher temperatures on the evaporation speed. Consequently, this more advanced setup would give an inside into the evaporation speed of (m)ethanol. Thus, it could be used to validate the single-droplet evaporation model.

References

[1] UK Research and Innovation. Shipping industry reduces carbon emissions with space technology. https://www.ukri.org/news/shipping-industry-reduces-carbon-emissions-with-space-technology/, 2021.

[2] International Maritime Organization. Initial imo ghg strategy. https://www.imo.org/en/MediaCentre/HotTopics/Pages/Reducing-greenhouse-gas-emissions-from-ships.aspx, 2018.

[3] DNV. Future fuels. https://www.dnv.com/maritime/hub/decarbonize-shipping/fuels/future-fuels.html.

[4] L. van Biert, M. Godjevac, K. Visser, and P. V. Aravind. A review of fuel cell systems for maritime applications. *Journal of Power Sources*, 327, 2016.

[5] R.G. van de Ketterij. Impact of methanol on the combustion process - an experimental study, 2020.

[6] Methanol Institute. Measuring maritime emissions - policy recommendations regarding ghg accounting of the maritime industry. https://www.methanol.org/wp-content/uploads/2020/04/Methanol-Institute-Measuring-Maritime-Emissions-Policy-Paper-August-2021.pdf, 2020.

[7] R. Edwards, J-F. Larivé, D. Rickeard. Well-to-tank report 4.a – jrc well-to-wheels analysis, 2014.

[8] DNV GL. Methanol as marine fuel: Environmental benefits, technology readiness, and economic feasibility, 2016.

[9] C.J. van Iersel. Injection and evaporation of 100% methanol – experimental and simulation-based research into the injection and evaporation of 100% methanol for use in a port-injected spark-ignited ice. https://repository.tudelft.nl/islandora/search/?collection=education, 2022.

[10] R.S. Tol. Combustion of diesel/methanol blends in a compression ignited engine. https://repository.tudelft.nl/islandora/object/uuid%3A51d875d8-19cf-4397-8755-680de1cbc080?collection=education, 2020.

[11] J.J. Bosklopper. Experimental and simulation based investigation of the performance of a 100% methanol port-injected spark-ignited engine. https://repository.tudelft.nl/islandora/object/uuid%3A946dbdf6-ea99-4f57-8441-5a012e704d37?collection=education, 2020.

[12] Avinash Kumar Agarwal, Anirudh Gautam, Nikhil Sharma, and Akhilendra Pratap Singh. *Methanol and the Alternate Fuel Economy*. Springer, 2019.

[13] John B. Heywood. *Internal Combustion Engine Fundamentals*. McGraw-Hill Education, 1988.

[14] Wugao Zhang, Xiaoling Chen, Genxiang Gu, Huaili Hu, Taotao Liu, and Zhen Huang. Experimental study of the spray characteristics of usld, methanol and dme on the swirl nozzle of a stirling engine. *Fuel Processing Technology*, 119, 2014.

[15] Sanghoon Lee and Sungwook Park. Experimental study on spray break-up and atomization processes from gdi injector using high injection pressure up to 30mpa. *International Journal of Heat and Fluid Flow*, 45, 2014.

[16] Wei Zeng, Min Xu, Gaoming Zhang, Yuyin Zhang, and David J. Cleary. Atomization and vaporization for flash-boiling multi-hole sprays with alcohol fuels. *Fuel*, 95, 2012.

[17] Min Xu, Yuyin Zhang, Wei Zeng, Gaoming Zhang, and Ming Zhang. Flash boiling: Easy and better way to generate ideal sprays than the high injection pressure. *SAE International Journal of Fuels and Lubricants*, 6, 2013.

[18] Anupam Ghosh, Prasad Boggavarapu, and R. V. Ravikrishna. Measurement of liquid and vapor penetration of evaporating methanol sprays. *Atomization and Sprays*, 30, 2021.

[19] L. Dodge and D. Naegeli. Injector spray characterization of methanol in reciprocating engines. *Southwest Research Institute*, 1994.

[20] André Morais Ferreira, Erika Kajino, Raul Maia, Rodrigo Salvio, and Vinicius Bertucci Augusto. Development of 1d simulation model of fuel injector for pfi application. *XXV Simpósio Internacional de Engenharia Automotiva*, 2017.

[21] Niculescu Titu. *Chapter 2: Study of Inductive-Capacitive Series Circuits Using the Simulink Software Package*. Technology and Engineering Applications of Simulink, 05 2012.

[22] Dariusz Szpica and Michał Kusznier. Modelling of the low-pressure gas injector operation. *Acta Mechanica et Automatica*, 14, 2020.

[23] Jiyuan Zeng. Modelling and simulation of the diesel engine injection systems. https://repository.tudelft.nl/islandora/object/uuid%3A8327c564-ba20-47ff-91d5-b6ce1f05bdbe, 2019.

[24] N. H. Chung, B. G. Oh, and M. H. Sunwoo. Modelling and injection rate estimation of common-rail injectors for direct-injection diesel engines. *Proceedings of the Institution of Mechanical Engineers, Part D: Journal of Automobile Engineering*, 222, 2008.

[25] Joel Alroe, A Prof T Farrell, and S Psaltis. Modelling the evaporation of a liquid droplet. *National Collaboration in the Mathematical Sciences*, 2013.

[26] R Byron Bird, Warren E Stewart, and Edwin N Lightfoot. Transport phenomena, revised 2nd edition. *John Wiley & Sons, Inc.*, 2006.

[27] G S H Lock. Latent heat transfer: An introduction to fundamentals, by g.s.h. lock, oxford university press, uk (1994). 288 pages. isbn 0-19-856284-5. *Developments in Chemical Engineering and Mineral Processing*, 5, 2008.

[28] Purdue University. Deviations from ideal gas law behaviour. https://chemed.chem.purdue.edu/genchem/topicreview/bp/ch4/deviation5.html.

[29] J. Crank. *The mathematics of diffusion. 2nd Edn.* London: Oxford University Press, 1979.

[30] S. V. Patankar. *Numerical heat transfer and fluid flow.* McGraw-Hill Education, 1980.

[31] A. J.H. McGaughey and C. A. Ward. Temperature discontinuity at the surface of an evaporating droplet. *Journal of Applied Physics*, 91, 2002.

[32] Hibbeler R. C. *Fluid mechanics*. Pearson, 2015.

[33] R. de Kat. Tstl 28 oktober 2020 – opgave 5: Uitwendige stromingen, 2020.